Thermal Effects in Interplanetary Spacecraft: The Pioneer Anomaly

F. Francisco[1]
Instituto Superior Técnico,
Av. Rovisco Pais 1, 1049-001 Lisboa, Portugal
(Dated: December 10, 2009)

We present a methodology based on point-like Lambertian sources that enables a reliable and comprehensive estimate of the overall thermally induced acceleration of the Pioneer 10 and 11 spacecraft. We show that, by developing a sensitivity analysis of the several parameters of the model, that one may achieve a valuable insight on the possible thermal origin of the so-called Pioneer anomaly.

I. INTRODUCTION

A. General Background

The existence of a Sun-bound anomalous acceleration on the Pioneer 10 and 11 spacecraft with a magnitude of $a_{\rm Pio} = (8.74 \pm 1.33) \times 10^{-10}$ m/s^2 has been put forward about a decade ago [1], and subsequently confirmed by two independent analyses [2, 3].

An effort was made to account for all known systematic effects that could introduce an error in the overall acceleration determination process, described in detail in Ref. [4]. An estimate of the bias and uncertainty introduced by each effect is found in Table I, including internal, external and computational systematics. This constitutes a baseline for the orders of magnitude of the various effects involved. At this point none of those contributions could account for the reported anomaly.

However, an unambiguous description of the anomaly is not yet available. For example, the distances at which the originally available Doppler measurements were conducted do not allow a clear discrimination between an acceleration towards the Sun or the Earth. It has also been shown that a signature characterised by a linear decay with a time constant larger than 50 years is also compatible with the anomaly data [2].

Other sources for anomalous effects have since been discarded, including the possibility that the Kuiper Belt's gravity may induce the reported acceleration. This would require a mass about two orders of magnitude higher than the commonly accepted value of $M_{\rm KB} = 0.3 M_{\rm Earth}$ [5].

It has also been suggested that a v^2 dependent drag force could account for the anomaly. However, a straightforward calculation shows that the environment density would have to be of order 10^{-19} g/cm^3 (*cf.* Ref. [5]). For comparison, the density of interplanetary dust is below 10^{-24} g/cm^3, while the density of interstellar dust (directly measured by the Ulysses spacecraft) is even smaller, at about 3×10^{-26} g/cm^3 [5].

With the failure of conventional explanations, many proposals have been advanced to explain the anomaly as a previously undiscovered fundamentally physical effect. As two examples of theories put forward in this context, one can cite Scalar Field based models [6] and Scalar-Tensor-Vector Gravity [7] (for an extensive list, see Ref. [6]).

B. Thermal Effects

Although initially dismissed the hypothesis that the explanation for the Pioneer Anomaly lies in the reaction force due to thermal radiation has become increasingly controversial.

Several estimates were performed for the heat dissipation of several spacecraft components, presenting the argument that initial values underestimated these effects. Specifically, these claims focused on the thermal emissions from the heat dissipation louvers on the front of the main equipment compartment [8] and the two Radioisotope Thermal Generators (RTGs) [9].

It was further claimed that a combination of several sources could actually account for the anomalous acceleration [10]. In an attempt to confirm these claims, more recent and thorough studies are carrying out the task of carefully modelling the Pioneer probes, in order to reproduce all relevant thermal effects with a sufficient accuracy [11, 12].

This paper is a summary of the dissertation with the same title, where the first results of a method based on point-like radiation sources are presented. This work has also been published in Ref. [13]. As we shall see, the said method is compatible with previous studies.

II. SOURCE DISTRIBUTION METHOD

A. Motivation

As discussed in the previous section, a full characterisation of the anomalous acceleration observed in the Pioneer trajectories is not yet available. Furthermore, the technical and engineering details about the spacecraft's design and construction are scattered across different sources of variable reliability and accuracy. Finally, the behaviour and evolution of the materials when exposed to the environment of space for over 30 years

TABLE I. Error budget for the Pioneer 10 and 11, taken from Ref. [4].

Item	Description of error budget constituents	Bias (10^{-8} cm/s^2)	Uncertainty (10^{-8} cm/s^2)
1	Systematics generated external to the spacecraft:		
	a) Solar radiation pressure and mass	+0.03	±0.01
	b) Solar wind		$\pm < 10^{-5}$
	c) Solar corona		±0.02
	d) Electro-magnetic Lorentz forces		$\pm < 10^{-4}$
	e) Influence of the Kuiper belt's gravity		±0.03
	f) Influence of the Earth orientation		±0.001
	g) Mechanical and phase stability of DSN antennae		$\pm < 0.001$
	h) Phase stability and clocks		$\pm < 0.001$
	i) DSN station location		$\pm < 10^{-5}$
	j) Troposphere and ionosphere		$\pm < 0.001$
2	On-board generated systematics:		
	a) Radio beam reaction force	+1.10	±0.11
	b) RTG heat reflected off the craft	−0.55	±0.55
	c) Differential emissivity of the RTGs		±0.85
	d) Non-isotropic radiative cooling of the spacecraft		±0.48
	e) Expelled Helium produced within the RTGs	+0.15	±0.16
	f) Gas leakage		±0.56
	g) Variation between spacecraft determinations	+0.17	±0.17
3	Computational systematics:		
	a) Numerical stability of least-squares estimation		±0.02
	b) Accuracy of consistency/model tests		±0.13
	c) Mismodeling of maneuvers		±0.01
	d) Mismodeling of the solar corona		±0.02
	e) Annual/diurnal terms		±0.32
	Estimate of total bias/error	+0.90	±1.33

is unknown. No definitive statements can then be made about the origin of the Pioneer Anomaly.

In this context, the usefulness of a detailed Finite Element Analysis (FEA) is compromised by the unavailability of detailed engineering specifications and schematics. Such an analysis would require, not only a detailed knowledge of the engineering details, but also an accurate model of the thermal behaviour of each component. Still, there are at least two studies of this kind currently underway [11, 12], necessarily involving a large number of assumptions and compromising the reliability of the results.

For this analysis, the chosen method would have to be computationally light, fast and flexible. This would allow for a quick evaluation of different scenarios. The flexibility and speed of the method are key issues in coping with the scarcity of information and in the identification of the most important parameters. Also, the scalability of the method allows for the progressive construction of increasingly detailed models with a growing precision in the results.

The method chosen is based on a distribution of point-like radiation sources along the main emitting surfaces of the spacecraft and the analysis of how the emitted radiation is absorbed and reflected by other surfaces. This approach does not try to describe the behaviour of each internal component, but instead tries to capture the contributions of the main components of the spacecraft, namely the RTGs and the main equipment compartment, which are derived from the global thermal power aboard the probes, which is reasonably well known.

This particular approach is especially suited for this

problem. The temperature data is limited to the readings of six individual sensors inside the main compartment and two on the RTGs. That combined with the little knowledge about the optical properties of the used materials seriously reduces the accuracy, regardless of the adopted method. The approach here presented tries to base itself on the little solid and reliable information available.

It is emphasised that any study of this scope involves a large number of assumptions. Therefore, it is crucial to have the ability to quickly test a wide variety of scenarios and reach unambiguous conclusions about their plausibility. This sensitivity analysis is made significantly easier by the short computation times. In addition, the simplicity of the formulation keeps the involved physics transparent throughout the entire process, allowing the scrutiny of every step.

This is a less comprehensive approach when compared to an FEA model, but allows for a direct interpretation of results, easy adaptability, as well as quite short computation times.

In order to assess the self-consistency of the method, a set of test cases was performed. The choice for a point-like source approach should also be verified. This may be achieved by increasing the number of sources and observing the convergence of the relevant quantities and results. If satisfactory, one may safely assume that continuous surfaces and components can be suitably modelled by point-like sources and still reproduce the physical interplay between them. The purpose is, of course, to allow an extrapolation to the Pioneer vehicles.

B. Physical Formulation

Our method is based on a distribution of isotropic and Lambertian point-like sources. If W is the emitted power, the time-averaged Poynting vector-field for an isotropic source located at (x_0, y_0, z_0) is given by

$$\vec{S}_{\text{iso}} = \frac{W}{4\pi} \frac{(x - x_0, y - y_0, z - z_0)}{\left[(x - x_0)^2 + (y - y_0)^2 + (z - z_0)^2\right]^{3/2}}. \quad (1)$$

In the case of a Lambertian source the optical intensity of the radiation is constant and the energy flux is proportional to the cosine of the angle with the normal:

$$\vec{S}_{\text{Lamb}} = \frac{W \cos\theta}{\pi} \frac{(x - x_0, y - y_0, z - z_0)}{\left[(x - x_0)^2 + (y - y_0)^2 + (z - z_0)^2\right]^{3/2}}. \quad (2)$$

Typically, one uses isotropic sources to model point-like emitters and Lambertian sources to model surfaces. The Poynting vector field of the source distribution is, then, integrated over the illuminated surfaces in order to obtain the amount of energy illuminating these, and the force produced. The former is given by the time-averaged Poynting vector flux

$$E_{\text{ilum}} = \int \vec{S} \cdot \vec{n}\, dA = \\ = \int \vec{S}(\vec{G}(s,t)) \cdot \left(\frac{\partial \vec{G}}{\partial s} \times \frac{\partial \vec{G}}{\partial t} \right) ds\, dt, \quad (3)$$

where the function $\vec{G}(s,t)$ parameterises the relevant surface. The radiation illuminating the surface will produce a force along the normal vector to that surface. Integrating that force, i.e., the radiation pressure multiplied by the unitary normal vector, will give us the total force acting upon that surface. The radiation pressure is thus given by

$$P_{\text{rad}} = \frac{\alpha}{c} \vec{S} \cdot \vec{n}, \quad (4)$$

taking into account a radiation pressure coefficient $1 \leq \alpha \leq 2$. The case $\alpha = 1$ corresponds to full absorption while $\alpha = 2$ indicates full diffusive reflection.

The force can be obtained by integrating the radiation pressure along a generic surface

$$\vec{F}_{\text{Rad}} = \int \frac{\vec{S} \cdot \vec{n}}{c} \frac{\vec{S}}{||\vec{S}||}\, dA. \quad (5)$$

In objects that have a reasonably complex geometry (such as the Pioneer spacecraft) there will be shadows cast by the surfaces that absorb and reflect the radiation. The shadowing effect of the illuminated surfaces is calculated with this same expression and then subtracted to the force obtained for the emitting surface. The total result is the sum of all effects $\vec{F}_i$, force on the emitting surface, shadows and radiation pressure on the illuminated surfaces $\vec{a}_{\text{Th}} = \sum_i \vec{F}_i / m$.

C. Test Cases

A set of test cases was used to assess the validity of the approximations made throughout our study and the efficiency of the method. The ability to adequately represent the thermal radiation emitted from an extended surface by a small number of point-like sources, as opposed to having many small thermal radiating elements, is the main issue under analysis.

In these test cases, we consider a square emitting surface with 1 m^2 and compare the results for an increasing number of sources, with a constant total power. It is expected that the result will converge to the exact solution as the number of radiation sources increases.

In radiation emitting surfaces without any other illuminated surfaces, one finds that the force only depends on the emitted power. Integrating Eq. (5) with Lambertian sources, we obtain a force in the direction normal to the surface with a magnitude of $(2/3)W_{\text{surf}}/c$.

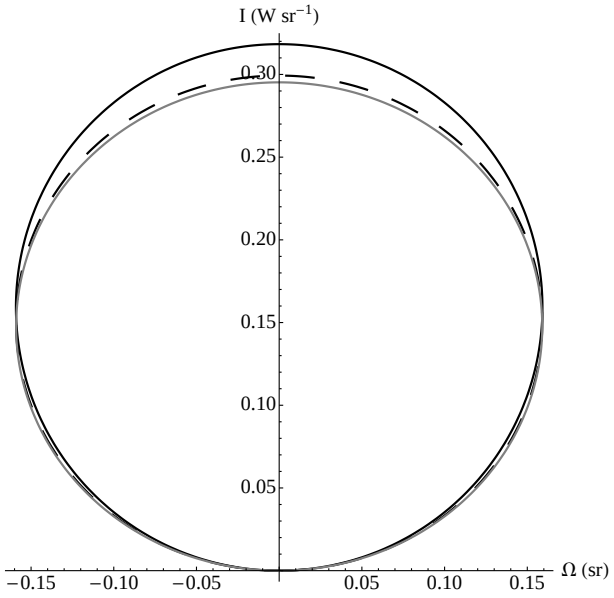

FIG. 1. Polar plot of the intensity variation with elevation of the radiation emitted by a surface on the $0xy$ plane (solid angle Ω), when considering 1, 4 and 16 Lambertian sources (full, dashed and grey curves, respectively), maintaining the total emitted power constant at 1 W (the curves for 64 or 144 sources overlap the one for 16 sources). The intensity at higher elevations (close to vertical) diminishes with the number of sources, compensating the slight increase at the lower angles.

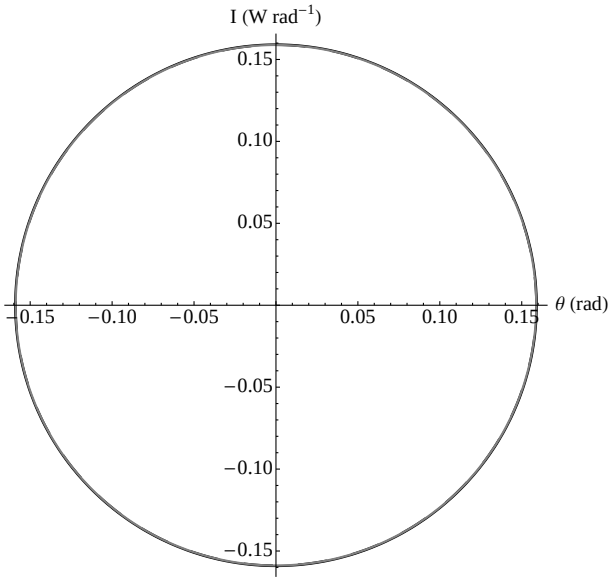

FIG. 2. Same as Fig. 1 but for intensity variation with azimuthal angle θ. All lines are superimposed, confirming that the total power is maintained constant.

In order to acquire some sensibility on that dependence of the modelled radiated energy field with the mesh used to represent the surface, we plot the variation of the radiation intensity with the elevation and the azimuth for 1, 4, 16, 64 and 144 source meshes, as depicted in Figs. 1 and 2.

A visual inspection of the results indicates that the highest deviation occurs at the higher angles of elevation and is less than 10%, even when comparing the roughest (1 source) with the finest mesh (144 sources). The deviations are expected to be smaller than that for the typical angles of the Pioneer spacecraft configuration.

In order to confirm this assumption, the force acting on a second 1 m^2 surface for several different positions is computed. A total of nine representative configurations were considered, centred in different positions and with several tilt angles, as summarised in Table II. The deviation between the results for 1, 4, 16, 64 and 144 source meshes is then verified.

As predicted, results show that the highest deviations occur with the second surface set at the highest elevation angle. Specifically, Test Case 8, depicted in Fig. 3, exhibits the highest variations in the results. The results in Table III show a difference of approximately 6% between the force obtained with one source and the results for the finer meshes (16, 64 and 144 sources). Still, the latter are all within 0.5% of each other, while the intermediate 4 source mesh has a deviation of just 1.5%.

TABLE II. Positions considered for the second surface in test cases. The first (emitting) surface is in the $x-y$ plane centred at the origin. Considered distances between both surfaces are typical for the Pioneer spacecraft.

Test Case #	Surface Centre Position (m)	Surface Tilt Angle (°)
1	(2, 0, 0.5)	90
2	(2, 0, 1.5)	0
3	(2, 0, 1.5)	30
4	(2, 0, 1.5)	60
5	(2, 0, 1.5)	90
6	(1, 0, 2)	0
7	(1, 0, 2)	30
8	(1, 0, 2)	60
9	(1, 0, 2)	90

One may take Test Cases 1 and 3 as examples of the typical angles and distances involved in the Pioneer probe's configuration. For the first case, depicted in Fig. 4, the energy flux and force computation give us the results shown in Table IV. The analysis of these results shows that, for 16, 64 and 144 sources, the variation in the energy flux and force is less than 0.5%. As before, the difference to the finer meshes' results is less than 5% for 1 source and less than 1.5% for a 4 source mesh. The results in Table V for Test Case 3 show that the difference between a 1 source and a 144 source mesh results in a variation of less than 5%. The convergence is, as

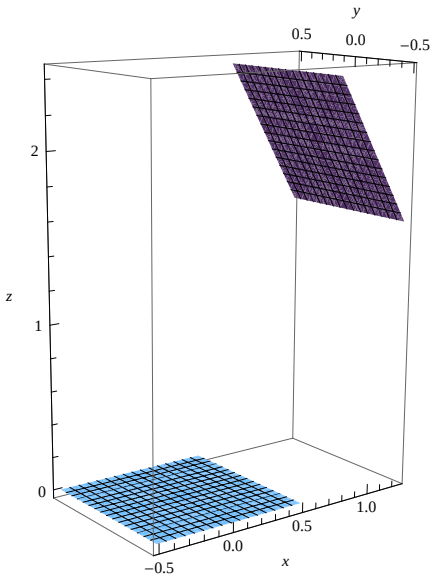

FIG. 3. Geometry of Test Case 8 (*cf.* Table II): thermal emission from a surface is simulated by a different number of Lambertian sources evenly distributed on the surface, maintaining the total emitted power constant, and the effect on a second surface is observed. This is the test case where the highest variation with the number os sources considered were obtained.

TABLE III. Results for Test Case 8 (*cf.* Table II) considering a total emission of 1 kW. As the number of sources to represent the thermal emission of a surface change, the resultant force components appearing by shadow on the secondary surface remain almost the same.

Sources	Energy Flux	Force components (x, y, z)
#	(W)	(10^{-7} N)
1	45.53	(2.016, 0, 2.083)
4	45.53	(1.918, 0, 2.003)
16	45.53	(1.895, 0, 1.984)
64	45.53	(1.890, 0, 1.979)
144	45.53	(1.889, 0, 1.978)

in both previous cases, achieved for the 16, 64 and 144 source meshes, with a variation of less than 0.25%.

In all the analysed test cases, convergence is achieved at a similar pace and always attaining small deviations. Ultimately, we conclude that a 4 source mesh, with deviations around or bellow 1.5%, would be adequate for the desired balance between precision and simplicity. The results of these test cases provide a fairly good illustration of the power of our method and how well we can estimate the radiation effects on the Pioneer probes. In particular, the deviation is always well below 10%, even with the roughest simplifications allowed by the chosen method. One may then conclude that, for the scales and geometry involved in the Pioneer Anomaly problem, the

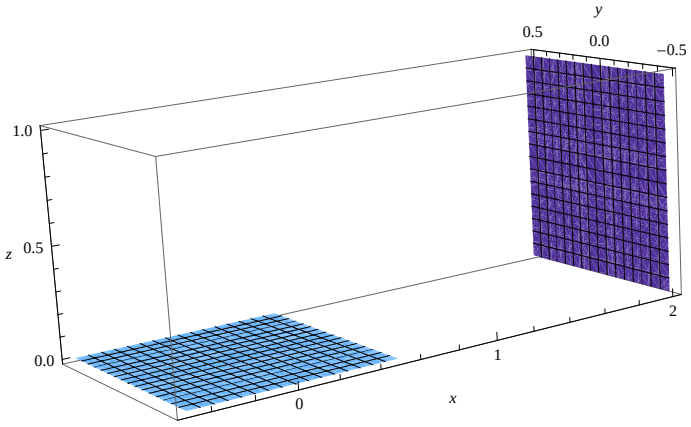

FIG. 4. Same as Fig. 3, for Test Case 1.

TABLE IV. Same as Table III, for Test Case 1.

Sources	Energy Flux	Force components (x, y, z)
#	(W)	(10^{-7} N)
1	15.34	(0.9300, 0, 0.1514)
4	15.92	(1.028, 0, 0.1638)
16	16.09	(1.038, 0, 0.1675)
64	16.13	(1.040, 0, 0.1684)
144	16.14	(1.041, 0, 0.1686)

source distribution method is, not only consistent and convergent, but that it provides an adequate estimate of the thermal radiation effects, bearing in mind all uncertainties involved.

Finally, after analysing the convergence of the method, we have also considered two additional test cases to assess the effect of ignoring minor surface features or geometric details, such as the equipment attached to the external walls of the spacecraft. The results indicate that, unless large temperature gradients are present, no significant errors will arise from considering flat surfaces and not taking into account all the details of the spacecraft.

III. THERMAL RADIATION MODEL OF THE PIONEER SPACECRAFT

A. Geometry

The introduction of some hypotheses can considerably simplify the task of modelling the Pioneer spacecraft. The first important fact to consider is the spin-stabilisation of the probes. If we further assume a steady-state thermal equilibrium through out most of the probes' journey, the time-averaged radial components of any force generated by anisotropic radiation will cancel along each revolution. Furthermore, the probe's axis of rotation (taken as the z-axis) is approximately pointing towards Earth, aligned with the approximate direction of

TABLE V. Same as Table III, for Test Case 2.

Sources #	Energy Flux (W)	Force components (x, y, z) (10^{-7} N)
1	19.20	(0.4952, 0, 1.037)
4	19.83	(0.5032, 0, 1.082)
16	19.99	(0.5050, 0, 1.093)
64	20.03	(0.5054, 0, 1.096)
144	20.04	(0.5055, 0, 1.096)

the anomalous acceleration.

A simplified version of the spacecraft geometry, retaining only the most important features, is considered in this study. The modelled configuration is depicted in Figs. 5 and 6. The components included in the model are the two cylindrical RTGs, a prismatic equipment compartment and the high-gain antenna (a paraboloid parametrized in cartesian coordinates by the function $\vec{G}(s,t) = \big(s,\ t,\ a(s^2+t^2)\big)$, with a parabolic coefficient $a = 0.25\ \mathrm{m}^{-1}$). Dimensions are taken from the available Pioneer technical drawings.

The results are obtained through the integration of the emissions of the RTG and lateral walls of the equipment compartment along the visible portion of the antenna. Radiation emitted from the front surface (facing away from the sun) of the equipment compartment doesn't illuminate any other surfaces. The back surface of the compartment, facing the antenna, will be discarded as its contribution is expected to be small for obvious geometric reasons: escaping radiation will be attenuated by multiple reflections between these two components and will be mainly in the radial direction, not contributing significantly to the anomalous acceleration. The antenna itself is expected to have a very low temperature with an approximately uniform distribution, not only axially, but also when comparing the front and back surfaces of the paraboloid. Therefore, its contribution can be regarded as negligible, with the surface acting solely as a reflector for the incoming radiation.

As we shall see, this simplified model captures the most important contributions to the thermal reaction force. The RTGs and the main equipment compartment are actually responsible for the vast majority of the emitted thermal radiation. In the case of the equipment compartment, an important contribution should come from the louvers located in the front wall, with consequences for the total power distribution.

B. Point-like Source Distribution

The thermal effects estimate results from a separate analysis of the three main contributions.

The front wall of the probe, where the louvers are located, is perpendicular to the axis of rotation. Its contribution thus corresponds to a force $(2/3)W_{\mathrm{front}}/c$ pointing in the Sun-ward direction along the probe's z-axis.

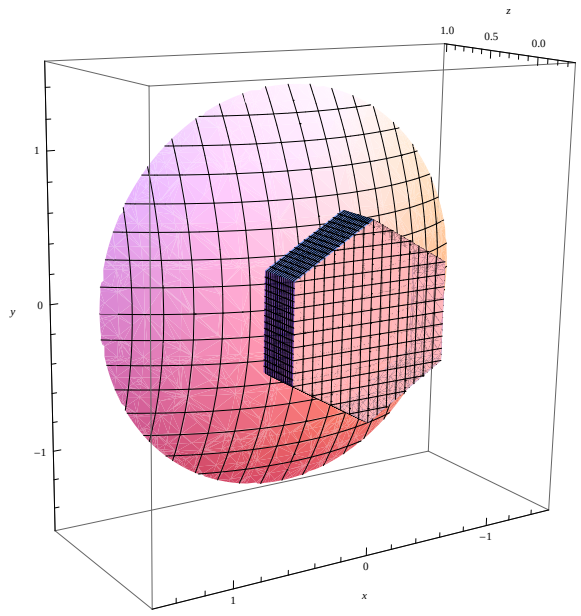

FIG. 5. Pioneer spacecraft model geometry considered in calculations, back view: high gain antenna and hexagonal main bus compartment.

The contribution from the side walls of the main compartment is obtained from the integration of the shadow and radiation pressure components along the antenna. The shadow of the RTGs is neglected due to their small size and relatively distant position, and the fact that most of its effect would be in the radial direction.

Following an analogous approach to the one used in the test cases, a convergence analysis was performed for the side walls of the main compartment. The results converge fairly quickly and the deviations are all below 2.5%, confirming the consistency previously demonstrated in our test cases. The obtained values show that between 16.8% to 17.3% of the power emitted from the side walls of this compartment is converted into a sun-ward thrust along the z-axis.

It is also important to check the effect of temperature gradients in the result. This is simulated by varying the relative power of the point-like sources in each surface, keeping the total power attributed to the surface constant. A variation of 20% in power between sources (simulating a 5% temperature variation) gives no significant changes in the final result, with relative differences smaller than 1%.

Finally, the RTG contribution is computed through two different models. In the first simpler scenario each RTG is a single isotropic source with the emissive power of the RTG itself. In the second model, the cylindric shape of the RTG is taken into account and a Lambertian source is placed at each base. It is only necessary to consider the source facing towards the centre of the spacecraft, as the remaining RTG radiation will be emitted ra-

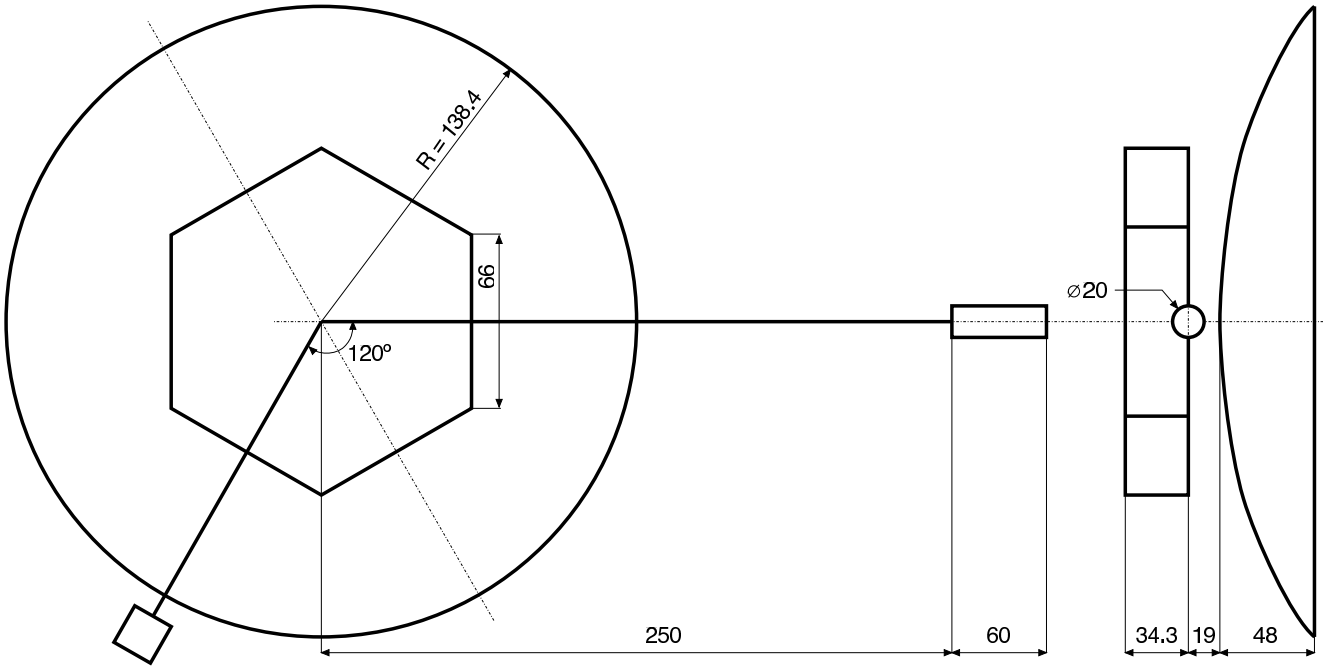

FIG. 6. Schematics of our simplified model of the Pioneer spacecraft, with relevant dimensions (in cm); second RTG and truss are not represented to scale, for convenience. Lateral view indicates the relative position of the RTGs, box compartment and the gap between the latter and the high gain antenna.

dially and its time-averaged contribution will cancel. In this case, the Lambertian source has a certain amount of the total RTG power, as discussed in the following sections. Depending on the model considered, either 1.9% of the total power or 12.7% of the power emitted from the base of the cylinder (equivalent to approx. 2% of total RTG power, if the temperature is uniform) is converted into a Sun-ward thrust.

These preliminary results do not take into account diffusive reflection, as allowed by Eq. 4. In the subsequent section, more accurate results will be presented and discussed.

C. Power Budget

From all the uncertainties involved in this study, the power data stands out as one of the few reliable pieces of information available. Furthermore, it is physically more consistent to consider the power instead of the temperature readings as it is the independent variable from which all estimates of the resulting thermal effects are derived.

The energy balance of the spacecraft in steady-state conditions relates the temperature T_i of a surface i with the power budget of the spacecraft

$$\dot{E}_{\rm absorb} + \dot{E}_{\rm gen} = \sum_i A_i \epsilon_i \sigma T_i^4, \tag{6}$$

where A_i are the relevant areas and ϵ_i the emissivity of each surface i.

All the power generated onboard the probes comes from the two plutonium-238 RTGs. The power conversion efficiency is quite low, and just a fraction is converted into electricity, the remaining power being dissipated as heat. Since the conduction effect through the RTG trusses can be considered negligible, it can be considered that all of the RTG thermal power is dissipated as radiation from the RTG itself.

The electrical power is consumed by the various instruments located in the main compartment, despite a considerable portion of it being used in radio transmissions from the high gain antenna.

As mentioned in Ref. [4], the total RTG thermal power at launch was 2580 W, producing 160 W of electrical power. This means that, at launch, approximately 2420 W of thermal power has been dissipated by the RTGs. Taking into account the plutonium decay with a half-life of 87.74 years, the total on-board power variation with time (in years) is given by

$$W_{\rm tot}(t) = 2580\ e^{(-\frac{t \ln 2}{87.74})}\ [\rm W]. \tag{7}$$

Telemetry data reveals that the electrical power decays at a faster rate than the plutonium radioactive decay; in the latest stages of the mission, about 65 W were available. Most of the electrical power is dissipated inside the main compartment. The electrical heat in the spacecraft body was around 120 W at launch, dropping to less than 60 W at the latest stages of the mission [11], following an approximate exponential decay with a half-life of

about 24 years. This difference in decay rates is mostly attributable to thermocouple degradation.

IV. RESULTS AND DISCUSSION

A. Order of Magnitude Analysis

Before the complete numerical estimate, one may use the results described above to perform a preliminary order of magnitude analysis. This establishes a frame of reference for the overall acceleration arising from thermal effects, which can be compared with the $a_{\rm Pio} \sim 10^{-9}$ m/s^2 scale of the Pioneer anomaly.

From the spacecraft specifications, one has a total mass $m_{\rm Pio} \sim 230$ kg, and separate RTG and equipment compartment powers $W_{\rm RTG} \sim 2$ kW and $W_{\rm equip} \sim 100$ W. As already discussed, the integration of the emissions of the RTG and instrument compartment indicate the proportion of emitted power that is effectively converted into thrust along the axial direction. Considering the simpler model discussed is section III B and the power emitted from each surface proportional to its area (equivalent to assuming uniform temperature and emissivity in the RTGs and equipment compartment), we obtain

$$\begin{aligned} F_{\rm RTG} &\sim 2\times 10^{-2}\frac{W_{\rm RTG}}{c},\\ F_{\rm sides} &\sim 10^{-1}\frac{W_{\rm equip}}{c},\\ F_{\rm front} &\sim 2\times 10^{-1}\frac{W_{\rm equip}}{c}. \end{aligned} \tag{8}$$

These values, divided by the spacecraft's mass, give us the acceleration:

$$\begin{aligned} a_{\rm RTG} &\sim 2\times 10^{-2}\frac{W_{\rm RTG}}{m_{\rm Pio}\,c} \sim 6\times 10^{-10}\ {\rm m/s^2},\\ a_{\rm equip} &\sim 3\times 10^{-1}\frac{W_{\rm equip}}{m_{\rm Pio}\,c} \sim 4.4\times 10^{-10}\ {\rm m/s^2}. \end{aligned} \tag{9}$$

This clearly indicates that both contributions are equally relevant to account for the reported anomalous acceleration of the Pioneer probes, as it shows that the RTGs and the instrument compartment yield similar thermal effects.

B. Thermal Force Estimate

Encouraged by the estimate outlined above, a more detailed evaluation of the existing thermal effects, using point-like source modelling, can now be undertaken.

A model with 4 sources in each side panel of the equipment compartment and Lambertian sources at the bases of the RTGs was chosen for this calculation, reflecting the discussion in section III B. This model has the best balance between accuracy and computation time (recall that the deviation of the source distribution relative to the finer meshes is less than 0.5%). Integrating the radiation pressure and shadow components using the methodology presented in section II B and extracting the axial component, we obtain an expression that yields the thermal acceleration

$$a_{\rm Th} = \frac{0.168W_{\rm sides} + \frac{2}{3}W_{\rm front} + 0.128W_{\rm RTGb}}{c\ m_{\rm Pio}} \tag{10}$$

where $W_{\rm sides}$ and $W_{\rm front}$ are the powers emitted from the side panels and front of the equipment compartment and $W_{\rm RTGb}$ is the power emitted from the base of the RTG facing the centre of the spacecraft. Remaining contributions are discarded at this point.

Keep the spacecraft geometry in mind, this expression reveals that all considered contributions yield a sun-ward acceleration. The $W_{\rm front}$ component radiates directly in a direction away from the sun, while the other two components $W_{\rm sides}$ and $W_{\rm RTGb}$ radiate laterally, illuminating the high gain antenna. The question now resides in correctly estimating the emitted powers. We shall consider the 1998 readings, as found in the graph of Ref. [11], namely: $W_{\rm RTG} = 2050$ W and $W_{\rm equip} = 58$ W. These are the dissipated thermal powers at the RTG and equipment compartment.

The simplest scenario, with uniform temperature and optical properties (emissions proportional to the surface area, as in the previous section), leads to

$$\begin{aligned} W_{\rm sides} &= 21.75\ {\rm W},\\ W_{\rm front} &= 18.12\ {\rm W},\\ W_{\rm RTGb} &= 41.11\ {\rm W}, \end{aligned} \tag{11}$$

yielding an acceleration $a_{\rm Th} = 3.05\times 10^{-10}$ m/s^2. This equates to around 35% of the anomalous acceleration. It should be noted that, considering the available temperature maps from Ref. [11], we see that the temperature anisotropies along the sides of the equipment compartment fall within the tested cases. However, the RTG temperature distribution should deserve a more careful analysis, as there are significant temperature changes between the wall of the cylinder, the bases and the fins. In addition, it is expected that the front wall of the equipment compartment will have a larger contribution than the side walls, due to the presence of the louvers.

If we consider that the louvers are closed and have a similar emissivity to the rest of the equipment platform, we can obtain the variation of the acceleration with the temperature ratio between the louvers and the mean temperature of the platform, while keeping the total power constant. This is depicted in Fig. 7. A similar analysis may be performed for the RTGs, considering the ratio between the temperatures at the base of the cylinder and the fins (Fig. 8).

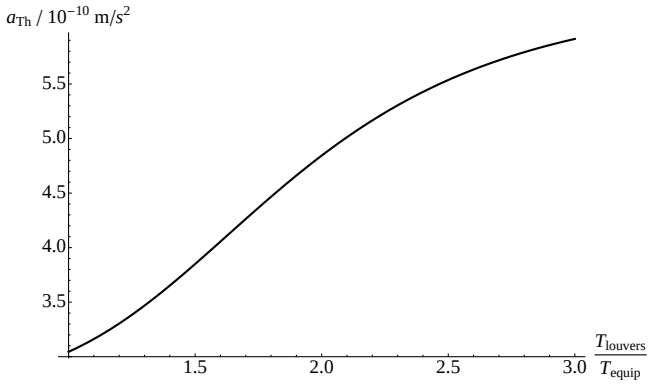

FIG. 7. Variation of the resulting acceleration with the temperature ratio between the louvers and the equipment platform, considering similar emissivities for both multi-layer insulations.

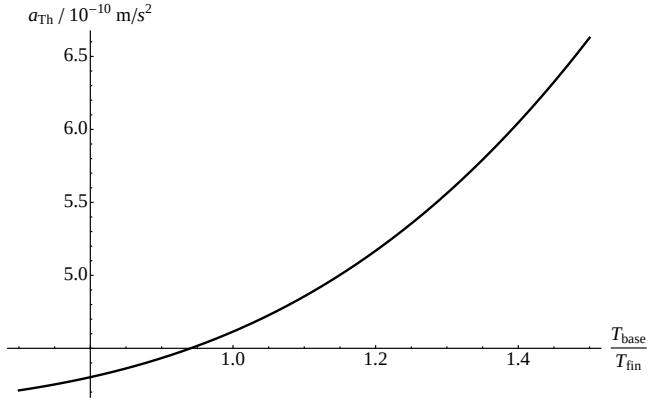

FIG. 8. Variation of the resulting acceleration with the temperature ratio between the base of the RTG cylinder and the fin temperature.

A second estimate can then be made, considering the RTG cylinder bases and wall as having a 15% and 30% higher temperature than the fins, respectively. Assuming also that the closed louvers have similar emissivities, although a 100% higher temperature than the rest of the equipment compartment could be possible, one obtains the following values for the powers:

$$\begin{aligned} W_{\rm sides} &= 9.97 \text{ W}, \\ W_{\rm front} &= 39.71 \text{ W}, \\ W_{\rm RTGb} &= 49.67 \text{ W}. \end{aligned} \tag{12}$$

In this case, 57% of the anomalous acceleration can be accounted for, that is, $a_{\rm Th} = 5.00 \times 10^{-10}$ m/s^2.

So far, our results do not take reflections into account, *i.e.*, full absorption of the radiation by the illuminated surfaces. In this study, we shall introduce diffusive reflection by assigning a value to the α parameter in Eq. (4). For the aluminium used in the construction of the antenna, the reflectivity is, typically, around 80% for the relevant wavelengths, yielding $\alpha = 1.8$. For the multilayer insulation of the equipment platform, a value of $\alpha = 1.7$ is considered. In these conditions, the illumination factors in Eq. (10) are modified to account for the reflection. With the same temperature conditions as in the previous case, the resulting acceleration is $a_{\rm Th} = 5.75 \times 10^{-10}$ m/s^2 – approximately two thirds of the anomalous acceleration.

The results presented in this section give us a fairly good idea of the changes involved when considering different hypotheses and parameters. The three discussed scenarios here illustrate how one can use our method to identify the most sensitive parameters and quickly assess the effect of the existing uncertainties, pointing the path where models must be refined for increasing the certainty of the results.

V. CONCLUSIONS

The presented work puts forward a method to estimate the acceleration of the Pioneer spacecraft due to thermal effects, based on point-like Lambertian sources. The flexibility and computation simplicity of the method allow for a reliable and fast estimate of the acceleration due to the various thermal contributions of the spacecraft components. This is sharply contrasting with the complexity and computationally demanding nature of the finite element analyses. Our methodology is potentially useful for a thorough parametric study of the various thermal contributions, as discussed in sections III and IV.

The discussed method displays a reasonable degree of accuracy, with a direct numerical computation error of the order of 10^{-14} or less, and deviations due to the approximation of the geometry with point-like sources falling below 1% (as argued in Sections II C and III B). However, it should be emphasised that this is not a direct indication of the accuracy of the actual thermally induced acceleration, when compared to the reported case of the Pioneer anomaly, but a measure of self-consistency of the developed method. The aim here is to demonstrate the reliability of the procedure, which should be extended in order to better simulate the physical system of the Pioneer spacecrafts, while keeping the flexibility and computational speed that have motivated this complementary approach.

After identifying the main contributions for the power of the various components of the spacecraft (RTGs, antenna and equipment bus compartment), figures ranging from 35% to 57% of the anomalous acceleration disregarding reflection. Inclusion of reflection implies that one can account for about 67% of the anomaly.

The natural continuation of this work involves refinement of the geometrical modelling, including the specular component reflection. In addition, and perhaps more importantly, the identification of parameters that most determinately affect the final result, namely temperatures, emissivities and reflectivities of the various components, such as the louvers and the RTG case. In any case, our analysis already agrees with other preliminary results from thermal models based on finite element methods [12].

[1] John D. Anderson, Philip A. Laing, Eunice L. Lau, Anthony S. Liu, Michael Martin Nieto, and Slava G. Turyshev. Indication, from pioneer 10/11, galileo, and ulysses data, of an apparent anomalous, weak, long-range acceleration. *Physical Review Letters*, 81(14):2858–2861, Oct 1998.

[2] Craig B. Markwardt. Independent Confirmation of the Pioneer 10 Anomalous Acceleration. arxiv.org/gr-qc/0208046, 2002.

[3] Viktor T. Toth. Independent analysis of the orbits of pioneer 10 and 11. *International Journal of Modern Physics D*, 18(5):717–741, 2009.

[4] John D. Anderson, Philip A. Laing, Eunice L. Lau, Anthony S. Liu, Michael Martin Nieto, and Slava G. Turyshev. Study of the anomalous acceleration of pioneer 10 and 11. *Physical Review D*, 65(8):082004, Apr 2002.

[5] O. Bertolami and P. Vieira. Pioneer anomaly and the kuiper belt mass distribution. *Classical and Quantum Gravity*, 23(14):4625–4635, 2006.

[6] O. Bertolami and J. Páramos. The pioneer anomaly in the context of the braneworld scenario. *Classical and Quantum Gravity*, 21(13):3309–3321, 2004.

[7] J. R. Brownstein and J. W. Moffat. Gravitational solution to the pioneer 10/11 anomaly. *Classical and Quantum Gravity*, 23(10), 2006.

[8] Edward M. Murphy. Prosaic explanation for the anomalous accelerations seen in distant spacecraft. *Physical Review Letters*, 83(9):1890, Aug 1999.

[9] J. I. Katz. Comment on ıindication, from pioneer 10/11, galileo, and ulysses data, of an apparent anomalous, weak, long-range accelerationȷ. *Physical Review Letters*, 83(9):1892, Aug 1999.

[10] Louis K. Scheffer. Conventional forces can explain the anomalous acceleration of pioneer 10. *Physical Review D*, 67(8):084021, Apr 2003.

[11] Viktor T. Toth and Slava G. Turyshev. Pioneer anomaly: Evaluating newly recovered data. In Alfredo Macias, Claus Lammerzahl, and Abel Camacho, editors, *RECENT DEVELOPMENTS IN GRAVITATION AND COSMOLOGY: 3rd Mexican Meeting on Mathematical and Experimental Physics*, volume 977, pages 264–283. AIP, 2008.

[12] Benny Rievers, Stefanie Bremer, Meike List, Claus Lämmerzahl, and Hansjörg Dittus. Thermal dissipation force modeling with preliminary results for pioneer 10/11. *Acta Astronautica*, 06(009), 2009.

[13] O. Bertolami, F. Francisco, P. J. S. Gil, and J. Páramos. Thermal analysis of the pioneer anomaly: A method to estimate radiative momentum transfer. *Physical Review D*, 78(10):103001, 2008.